Journal of Power Sources 191 (2009) 144–148

Contents lists available at ScienceDirect

Journal of Power Sources

journal homepage: www.elsevier.com/locate/jpowsour

Short communication

Influence of Mg^{2+}, Al^{3+}, Co^{2+}, Sn^{2+} and Sb^{3+} on the electrical performance of doped β-lead dioxide

N. Chahmana [a], L. Zerroual [a,*], M. Matrakova [b]

[a] Laboratoire d'Energétique et Electrochimie du Solide (LEES), Université Ferhat ABBAS, Sétif 19000, Algeria
[b] Institute of Electrochemistry and Energy Systems (CLEPS), Bulgarian Academy of Sciences, Sofia 1113, Bulgaria

ARTICLE INFO

Article history:
Received 9 September 2008
Received in revised form 24 October 2008
Accepted 29 October 2008
Available online 7 November 2008

Keywords:
PAM
Gel zones
Nanoparticles
Doping
Battery electrical performance

ABSTRACT

The relationship between the hydrogen content of the crystal lattice of PbO_2 and the capacity of PAM is still a subject of interest. The present paper concerns the effect of the doping of β-lead dioxide on the composition of PAM gel zones and its relationship to battery performance.

Differential scanning calorimetry (DSC) and thermogravimetry (TG) as well as X-ray diffraction analysis were used as techniques of investigation in this study. The results showed that the quantity of water present in the gel zones and PAM discharge capacity are mainly dependant of the nature of the dopant.

1. Introduction

The positive lead dioxide active material (PAM) of lead acid batteries is formed by electrochemical oxidation of basic lead sulfates and lead oxide. The capacity of the positive plate depends mainly on the ratio between the two forms of lead dioxide α and β-PbO_2.

Pavlov [1] showed that lead dioxide active mass is a gel-crystal system with proton and electron conductivity. Mohanov et al. [2] found hydrated structures in the anodic layer formed on lead electrodes in H_2SO_4 solution. At a given potential, Pb^{4+} ions are formed on the electrode surface. These are unstable in water solutions and form $Pb(OH)_4$. The $Pb(OH)_4$ is dehydrated partially or completely giving $PbO(OH)_2$ and PbO_2. The electrode surface is covered by a layer of PbO_2, $PbO(OH)_2$ and $Pb(OH)_4$, which layer has gel-like properties.

According to Pavlov et al. [3] during discharge of the positive battery plate, the reduction of PbO_2 and $PbO(OH)_2$ to $PbSO_4$ proceeds in two stages. The first is electrochemical and occurs in the bulk of the agglomerates and particles and gives $Pb(OH)_2$. During the second stage, $PbSO_4$ formation takes place through a chemical reaction between $Pb(OH)_2$ and H_2SO_4.

In our previous work [4], using an all solid state system exempt of H_2SO_4, the kinetic tests and coulometric data show that the process of PAM reduction includes two electrochemical stages (one electron is consumed during each stage) taking place in the gel zones according to a proton-electron mechanism or a double-injection process. The role of structural water in the reactivity of the positive active mass has been emphasized by different authors [5–13]. They concluded that the heat treatment of PAM reduces the discharge capacity and decreases considerably the proton diffusion coefficient.

The effects of metal ions addition in the electrolyte and in the grid alloys on the battery electrical performance have been investigated by several authors [14–21]. The objective of the present paper is to determine the impact of the following ions (Mg^{2+}, Al^{3+}, Co^{2+}, Sn^{2+} and Sb^{3+}) on the properties of the active material of positive battery plates.

2. Experimental

2.1. Materials

The paste was prepared in a mixer at 35 °C from leady oxide (72% PbO). The XRD pattern of the starting material showed the presence of tetragonal PbO and Pb. Leady oxide (LO) was mixed with water and 1.40 s.g. H_2SO_4 in a ratio equal to 5% H_2SO_4/LO. β (ND: non doped sample) and doped β lead dioxide were prepared by electroformation of cured battery plates (with grids cast from a Pb-5 wt.% Sb alloy) in acidic solution according to the method described by Voss and Freundlich [22]. The dopants were dissolved

* Corresponding author. Tel.: +213 36 92 51 21; fax: +213 36 92 51 33.
E-mail address: zerroual@yahoo.fr (L. Zerroual).

0378-7753/$ – see front matter © 2008 Elsevier B.V. All rights reserved.
doi:10.1016/j.jpowsour.2008.10.115

in the solution as sulfate salts, antimony was added as Sb_2O_3 oxide. The initial concentration of each dopant is 10^{-3} M. Analytical grade reagents and distilled water were used for all solutions. After washing in running water for several hours to remove excess of sulfuric acid, the plates were dried overnight at 110 °C. A part of the active mass was removed from the grids and ground to powder. This powder was placed in a glass flask and then used for X-ray diffraction, thermal and chemical analyses.

2.2. XRD sample characterisations and chemical analysis

The positive active materials were characterized by XRD analysis using an APD-15 Philips 2134 diffractometer. The relative intensity of the X-ray characteristic diffraction lines was adopted as a measure of the phase changes in the positive active material. It is defined as the ratio of the 'i' phase characteristic reflection intensity and the sum of the intensities of the characteristic diffraction lines of all phases. PbO_2 and $PbSO_4$ in PAM were respectively determined by volumetric titration with $KMnO_4$ solution and gravimetric precipitation with 5% $BaCl_2$ solution, the total Pb was determined by atomic absorption method. The amount of PbO in PAM was deduced from the difference between the total Pb and the sum of PbO_2 and $PbSO_4$ contents. Analytical grade reagents and twice distilled water were used for all solutions.

2.3. Thermal analysis

All tests were performed using instruments supplied by Mettler Toledo: DSC 822e and TGA/SDTA 851e. All measurements were carried out in Nitrogen atmosphere at a gas flow-rate of 80 $cm^3\ min^{-1}$ for DSC and 50 $cm^3\ min^{-1}$ for TGA at constant heating rate of 2 K min^{-1} for doped and 10 K min^{-1} for non doped sample. All materials were dried at 60 °C to evaporate the surface absorbed water.

2.4. Electrochemical investigations

The electrochemical measurements were carried out in a three-electrode cell. The working electrode with an apparent surface area of 0.7 cm^2 is at 1 cm distance from two large platinum rectangular-shaped counter electrodes. An Hg/Hg_2SO_4/saturated K_2S0_4 reference electrode was used. The potential-current curves were recorded after cycling the electrodes in 1.28 s.g. H_2SO_4 solution in the potential range 1.4 to 0 V at a sweep rate of 100 mV s^{-1}. The capacity expressed in mAh cm^{-2} is determined by integrating the surface area of the cathodic peak corresponding to the reduction of PbO_2 to $PbSO_4$. Non doped and Tin and Antimony doped electrodes were discharged at a constant cathodic current of −10 mA and the electrode potential versus capacity was recorded. The discharge capacity is expressed in mAh g^{-1}. All experiments were carried out at room temperature.

3. Results and discussions

3.1. Samples characterizations

Table 1 summarizes the obtained results for the chemical composition of the PAM samples formed in solutions with different dopants. The data show that traces of $Mg^{2+}$and Al^{3+} are present in the active mass, whereas important quantities of Sn^{2+}, $Co^{2+}$and $Sb^{3+}$are found. This affects the chemical composition of the positive mass. The amount of PbO_2 decreases, whereas that of PbO increases. In addition, small quantities of unconverted $PbSO_4$ is found in the majority of the samples.

Fig. 1 shows the XRD spectra for doped and non doped samples. All detected peaks were identified to be β-lead dioxide. Although

Table 1
Results from chemical and ICP-AES analyses of doped and non doped samples.

Samples	PbO_2	$PbSO_4$	PbO	% dopant (ICP-AES)
ND	93.59	1.93	3.26	
Mg^{2+}	87.57	3.25	7.31	0.0006
Al^{3+}	90.12	–	8.03	<0.0002
Co^{2+}	90.09	–	8.10	0.1
Sb^{3+}	87.72	1.73	8.48	0.02
Sn^{2+}	85.29	2.79	8.65	0.1

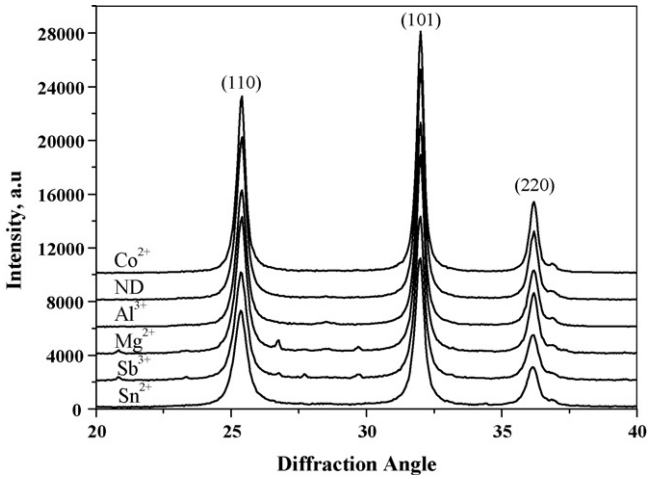

Fig. 1. XRD patterns of doped and non doped samples.

no differences in the spectra were observed, changes in peak intensity and width were clearly detected. As the result of comparison of the diffraction angles of non doped and doped PAM, it was found that the peaks of samples containing Sn^{2+}, Sb^{3+}, Mg^{2+}, and Al^{3+} shifted slightly to the high angle. In contrast, in the case of sample with Co^{2+} the peaks shifted to the low angle. This means that the interplanar distance changed and it suggests that the different cations were doped into β-PbO_2 crystal structure; as a consequence of this, it is considered that the particle diameter of PAM changed. The average crystallite size was calculated from the full width at the half maximum (FWHM) of [1 1 0] diffraction lines using Sherrer equation. The changes in crystallite size (%) thus calculated for the different dopants are reported in Table 2. The results showed an increase in the average crystallite size of the sample doped with Co^{2+}, whereas smaller particles of PbO_2 were obtained when the material is doped respectively with Al^{3+}, Mg^{2+}, Sb^{3+}, and Sn^{2+}.

Fig. 2 presents the intensities of the diffraction lines that correspond to the interplanar distances 3.50, 2.79 and 2.48 Å for β-PbO_2 measured for the different samples. It can be deduced that the sample doped with Co^{2+} exhibited high peak intensity with higher density active mass and higher crystallinity. PAM respectively doped with Al^{3+}, Mg^{2+}, Sb^{3+}, and Sn^{2+}showed a progressive decrease in the peak intensity. As a consequence of this, these dopants tend to diminish the crystallinity of PAM particles and

Table 2
Changes in crystal size calculated for doped and non doped samples.

Samples	Changes in crystallite size (%)
ND	–
Mg^{2+}	−10.90
Al^{3+}	−09.10
Co^{2+}	+18.2
Sb^{3+}	−22.70
Sn^{2+}	−27.30

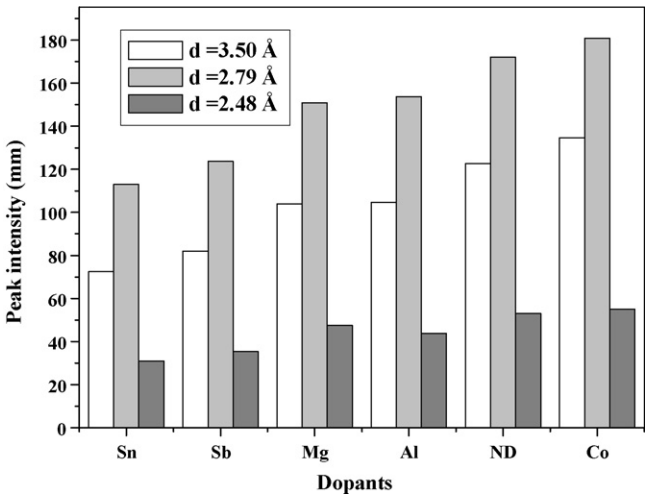

Fig. 2. Changes in intensity of characteristic diffraction lines for β-PbO_2 (d = 3.50 Å, d = 2.79 Å, d = 2.48 Å) in doped and non doped samples.

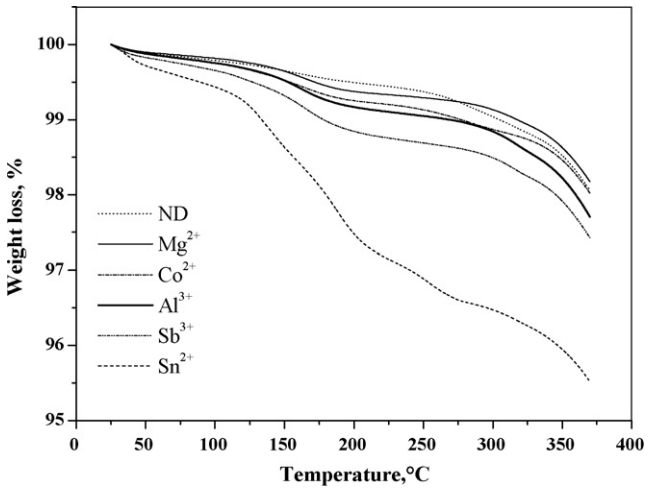

Fig. 4. Weight losses of the different materials as a function of heating temperature.

agglomerates and are in favour of gel formation with lower density active mass. These experimental findings confirm the changes in crystallite size reported in Table 2.

On heating the samples during the differential thermal gravimetric (DTG) measurements the gel zones decompose, hydrating water evaporates and the different samples lose weight depending on the nature of the dopant. Fig. 3 presents the obtained DTG curves calculated from the first derivative of TGA curves normalized toward mass. The DTG curve of non doped sample features three characteristic peaks at 125, 170 and 280 °C. These peaks are indicative of different types of water bonding in PAM gel zones. The dopants exert a remarkable increase in the peaks intensities and a slight shift towards high temperature is observed especially in the case of antimony and tin ions.

In Fig. 4 are represented the weight losses of the different materials as a function of heating temperature. The weight loss becomes greater when the PAM is doped respectively with Mg^{2+}, Co^{2+}, Al^{3+}, Sb^{3+}, and Sn^{2+}ions. This indicates that some hydration processes take place in the gel zones of PAM. The changes in H_2O content in the PAM (as measured by thermal gravimetry (TG)) for the doped and non doped samples, are reported in Fig. 5. The PAM dehydration occurs in three stages. Up to 100 °C, physisorbed water evaporates. In the temperature range comprised between 100 and 300 °C, chemisorbed water decomposes in two steps. An increase in total weight loss is observed with the doped samples. The water content respectively in antimony and tin doped PAM is more important as compared to all other samples. This result is in good agreement with the previous XRD data, the incorporation of tin and antimony in the PAM gel zones leads to a decrease in the crystallinity and small amorphous and hydrated particles are obtained.

On heating the samples at linearly increasing temperature the energy of dehydration was determined. Fig. 6 presents the DSC curves for doped and non doped samples. The PAM dehydration occurs between 25 and 300 °C and features an endothermic peak at 60 °C (indicative of physisorbed water evaporation) and two exothermic peaks respectively at 180 and 260 °C corresponding to chemically bonded water. The mechanism of dehydration is a charge exchange between hydroxyl groups OH^- and Pb^{4+} ions both present in the PAM gel zones according to Eq. (1):

$$2OH^- + Pb^{4+} \rightarrow Pb^{2+} + \tfrac{1}{2}O_2 + H_2O \quad (1)$$

On heating, $PbO(OH)_2$ amorphous parts in PAM are decomposed to PbO with H_2O and O_2 evolution according to Eq. (2):

$$PbO(OH)_2 \rightarrow PbO + \tfrac{1}{2}O_2 + H_2O \quad (2)$$

A broad exothermic peak with high intensity is observed in the case of sample doped with Sn^{2+}. This indicates the presence of great amount of structural water in this sample. The average dehydra-

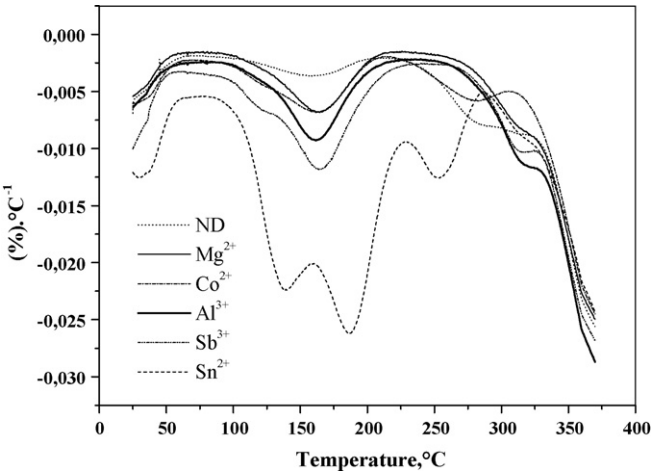

Fig. 3. DTG curves of doped and non doped samples.

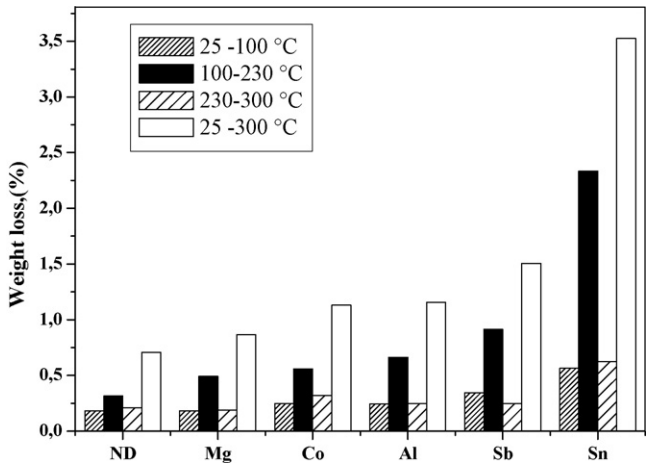

Fig. 5. Changes in water content for doped and non doped samples.

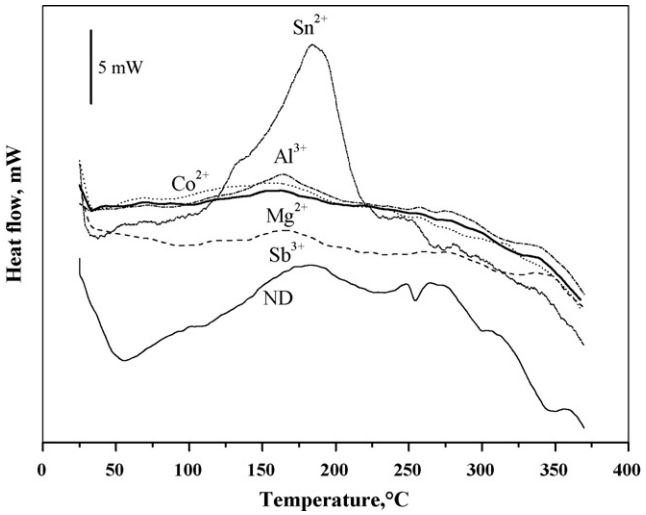

Fig. 6. DSC curves for doped and non doped samples.

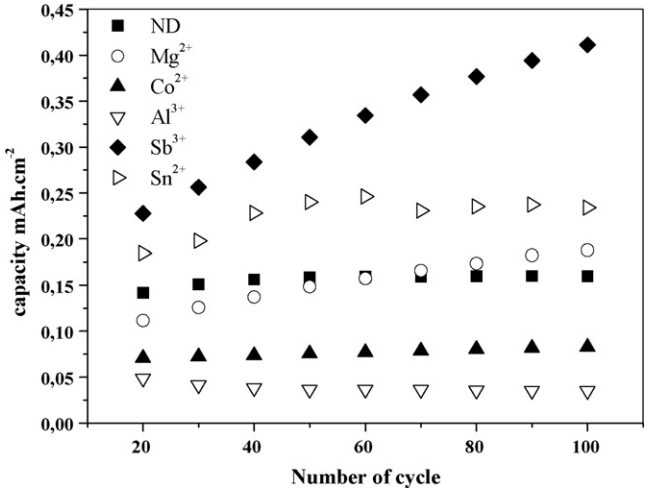

Fig. 8. PAM capacity vs. number of cycles for doped and non doped samples.

tion energies were calculated by integrating the surface area of the exothermic peak in the range of temperature comprised between 100 and 230 °C. The obtained values versus weight loss are presented in Fig. 7. A linear dependence between the energy and water content in the samples is observed except for the sample doped with Sb^{3+} that does not respect the linearity and gives small value of energy, although the great water content of this sample. This indicates that antimony doped PAM features quite different thermal properties. The incorporation of Sb^{3+} in the gel zones increases the contact between the polymer chains of amorphous lead dioxide. This means that agglomerates are connected to each other via antimony bridges to form uninterrupted polymer chains along which electrons move easily, the electrical conductivity is improved and the charge transfer from hydroxyl groups OH^- to Pb^{4+} is easier. As a consequence of this, less energy is needed to decompose $PbO(OH)_2$ amorphous parts in PAM.

3.2. Electrochemical properties

The electrochemical performance of the different samples was compared after cycling the electrodes in 1.28 s.g. H_2SO_4 solution. The PAM capacity versus the number of cycles for doped and non doped samples is presented in Fig. 8. We can see that the capacity of β-PbO_2 increases during the first cycles then reaches a stable value after the 40th cycle. Almost no difference is recorded with the non doped sample when Magnesium is considered except a slight increase in the capacity value during the last 20 cycles. In contrast, samples doped with Cobalt and Aluminium respectively decrease the capacity of PAM. Tin and antimony increase the capacity of PAM. Samples doped with tin present a similar profile as that of β-PbO_2. Sample doped with Antimony presents higher value of capacity and a linear increase with number of cycles is recorded.

The discharge curves of antimony and tin doped PAM are compared to that of β-PbO_2 in Fig. 9. We report the change in potential versus the capacity of the electrode expressed in mAh g^{-1}. Both tin and antimony are incorporated in β-PbO_2 gel zones and improve its electrochemical activity and electrical performance. We can see that tin and non doped sample present similar profile except a slight increase in the capacity value recorded for PAM doped with tin. In the contrary, antimony doped sample presents a high potential plateau and high capacity value as compared to the other samples. This result confirms the previous capacity values obtained when cycling the electrodes.

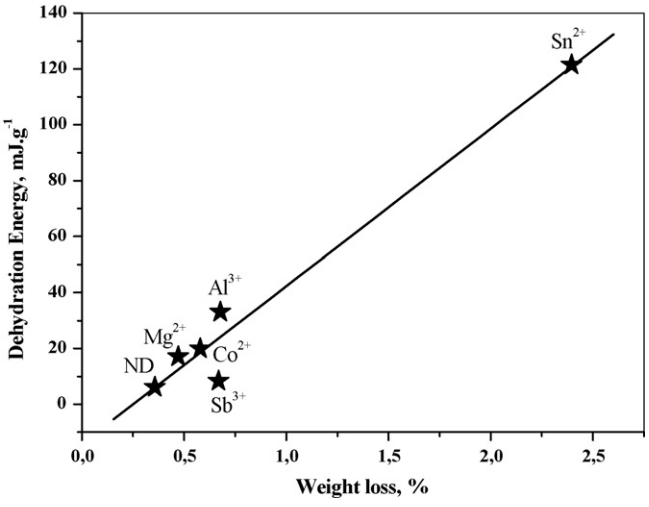

Fig. 7. Average dehydration energies vs. weight loss for doped and non doped samples.

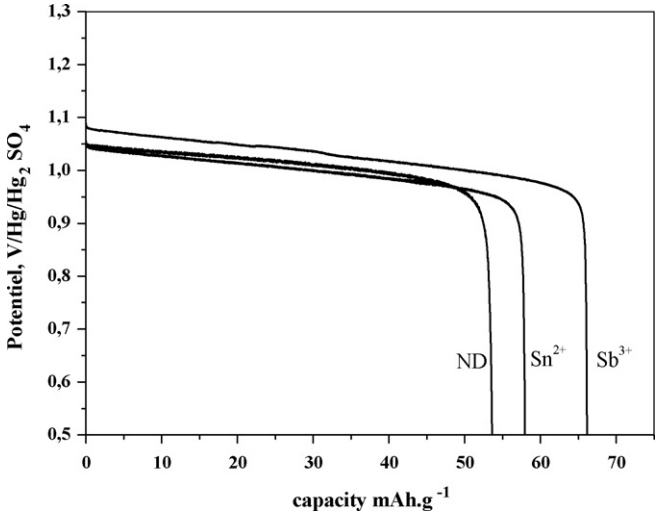

Fig. 9. Discharge curves of antimony and tin doped PAM compared non doped sample.

4. Conclusions

The experimental data obtained in this study are in general agreement that the incorporation of metallic ions in the gel zones of the positive active material influences its physico-chemical and electrochemical properties. The experimental findings showed that small quantities of magnesium and aluminium are introduced in PAM. In contrast, tin, antimony and cobalt were doped in β-PbO_2. The maximum admissible level of the metal ion depends on the nature of the dopant itself. The different ions affect the phase composition and the structural properties of the positive mass. As a consequence of this, the PbO_2/PbO ratio in the material is modified as well as water content. Tin and antimony doped samples present higher amounts of structural water and are in favour of the formation of amorphous and hydrated PbO_2 particles in the gel zones. The crystal size of the lead dioxide particles becomes significantly smaller, this leads to an increase in the area of the PAM and the connectivity between the polymer chains might be increased too. Thus, a great number of particles would be involved in the current generation process. As a consequence of this, the reaction area of the positive electrode and the total electrical contact area between the particles increase. An improvement in the capacity is observed with tin and antimony doped samples. This is a proof of the assumption that the capacity of PAM is determined by the electron conductivity of the gel zones. It seems that antimony affects more the gel conductivity comparing to tin, which curve is similar in profile to that of β-PbO_2. The later is reputed to present poor electronic conductivity. These experimental investigations should be taken in consideration in the process of lead-acid battery manufacture to improve the PAM capacity and power performance.

References

[1] D. Pavlov, J. Electrochem. Soc. 139 (1992) 3075.
[2] B. Mohanov, D. Pavlov, J. Appl. Electrochem. 23 (1993) 1244.
[3] D. Pavlov, I. Balkanov, P. Rachev, J. Electrochem. Soc. 134 (1992) 2390.
[4] R. Fitas, N. Chelali, L. Zerroual, B. Djellouli, Solid State Ionics 127 (2000) 49.
[5] R.J. Hill, M.R. Houchin, Electrochim. Acta 30 (1985) 559.
[6] I. Peterson, E. Ahlberg, J. Power Sources 91 (2000) 137.
[7] D. Pavlov, A. Kirchev, M. Stoycheva, B. Monahov, J. Power Sources 137 (2004) 288.
[8] R. Fitas, L. Zerroual, N. Chelali, B. Djellouli, J. Power Sources 64 (1997) 57.
[9] J. Morales, G. Petkova, M. Cruz, A. Caballero, J. Power Sources 158 (2006) 831.
[10] L. Zerroual, R. Fitas, B. Djellouli, N. Chelali, J. Power Sources 158 (2006) 837.
[11] U. Hullmeine, A. Winsel, E. Voss, J. Power Sources 25 (1989) 27.
[12] A. Winsel, E. Voss, H. Hullmeine, J. Power Sources 30 (1990) 209.
[13] E. Meissner, E. Voss, J. Power Sources 33 (1991) 231.
[14] B.K. Mahato, W.H. Tiedemann, J. Electrochem. Soc. 130 (1983) 2139.
[15] L.T. Lam, J.D. Douglas, R. Pilling, D.A.J. Rand, J. Power Sources 48 (1994) 219.
[16] H. Sanchez, Y. Meas, I. Gonzalez, M.A. Quiroz, J. Power Sources 32 (1990) 43.
[17] M. Maja, N. Penazzi, J. Power Sources 22 (1988) 1.
[18] K. Mc Gregor, J. Power Sources 59 (1996) 31.
[19] D. Pavlov, J. Power Sources 33 (1991) 221.
[20] D. Pavlov, A. Dakhouche, T. Rogachev, J. Power Sources 42 (1993) 71.
[21] D. Pavlov, J. Power Sources 46 (1993) 171.
[22] E. Voss, J. Freundlich, in: D.H. Collins (Ed.), Batteries, Pergamon, Oxford, 1963, p. 73.